XL CILAMCE
IBERO-LATIN AMERICAN CONGRESS ON COMPUTATIONAL METHODS IN ENGINEERING
NOVEMBER 11-14, 2019
Praiamar Natal Hotel & Convention Natal, RN-BRAZIL

AN ACCURATE AND EFFICIENT METHOD FOR STATIC ANALYSIS OF MARINE RISERS

Luana A. G. Moura
Juliana C. Alves
Evandro Parente Jr.
luanaandreza10@gmail.com
julianacunhalves@gmail.com
evandro@ufc.br
Laboratório de Mecânica Computacional e Visualização (LMCV), Departamento de Engenharia Estrutural e Construção Civil, Universidade Federal do Ceará
Campus do Pici, Centro de Tecnologia Bloco 728, 60455-760, Ceará/Fortaleza, Brasil
Ligia Tornisiello
ligiatornisiello@gmail.com
Louisiana State University
3304 Patrick F. Taylor Hall, Baton Rouge, LA 70803, United States

Abstract. Risers are essential components of offshore oil and gas production systems since they are responsible for transport these fluids to/from the wells from/to the floating facilities. Thus, structural analysis of marine risers has been an active research field in the last decades. Currently, there are many reliable analysis programs for riser analysis based on the Finite Element Method (FEM). However, this approach incurs in high computational costs due to its complexity and alternatives that are more efficient have been sought. Risers are subjected to static and dynamic loads, but it is known that in the earlier steps of riser design it is very important to evaluate the riser behavior under static loads, as self-weight, buoyancy, hydrostatic pressure, currents and floater movements (static offset). This paper presents an efficient and accurate approach for riser static analysis based on the numerical integration of the differential equilibrium equations of a cable subjected to vertical and horizontal static loads. The riser is modeled as an inextensible cable without bending stiffness, subjected to effective weight, drag force and offset. The riser behavior is governed by a nonlinear system of ordinary differential equations. The resulting nonlinear Boundary Value Problem (BVP) is solved using the Newton-Raphson Method with line searches to guarantee global convergence and increase efficiency. Initial values are estimated in order to transform the BVP in an initial value problem. The fourth-order Runge-Kutta method is used in the numerical integration of the resulting initial value problem. A post-processing procedure is used to evaluate the bending moment along the riser. This approach is suitable for analyzing analyze different riser configurations, such as steel catenary risers and lazy-wave risers. The accuracy and efficiency of the proposed approach are assessed and the results are compared with the FEM for different riser configurations. The results show that the presented approach is not only much more efficient than FEM but also can be more accurate.

1 Introduction

Risers are essential components of offshore production systems, since they connect the subsea units to the platforms, transporting fluids to/from the wells from/to the floating facilities. With the exploration and development of new oil and gas reservoirs located increasingly deepwater, the environmental conditions became more severe, leading to an increase in riser costs. When considering field development costs and technological feasibility, riser technology is a crucial issue [1].

Riser analysis aims to evaluate the geometry and internal forces along the riser due to the acting loads. Design standards use these results for assessment of riser integrity under burst, collapse and combined load criteria [2]. Different techniques have been proposed for riser analysis. Chakrabarti and Framptom [3] presented a review of techniques for riser analysis, which included different solution methods, such as finite differences and finite elements. Patel and Seyed [4] presented a review of proposed approaches for static and dynamic analysis of flexible risers. Currently, the Finite Element Method (FEM) is the standard analysis procedure for riser design, as it can accurately model the riser behaviour, including nonlinear and dynamic effects, environmental loads, riser-soil interaction and other complex phenomena. Several FE programs for riser analysis are available [5].

Several structural models with different fidelity degrees can be used for riser analysis. As a general rule, the computational cost of engineering simulations increases with the model fidelity. Thus, complex models base on the Finite Element Model (FEM) can simulate the static and dynamic behaviour of risers with great accuracy, but it incurs in high computational costs. In the initial steps of riser design, simpler models can be used to analyse the riser under static loads. In addition, there are many studies concerning riser design and optimization, and riser static response is one of the prerequisites in these studies [6].

During the optimization process, a high number of riser designs need to be evaluated, especially when genetic algorithms (GA) or other meta-heuristic methods are used. Thus, it is important to obtain the riser static response in an accurate and efficient manner. This raises the need for simple and representative models to perform these analyses. Lima et al. [7], Jacob et al. [8], Pina et al. [9] and Silva et al. [10] adopted simple models based on catenary equations in their studies. However, such models only consider vertical loads and are unable to account for the effect of sea currents.

Ghadimi [11] used a lumped spring-mass approach for the static and dynamic analyses, which considers vertical loads and estimates the bending moment from the approximate curvatures. The lumped-mass model was employed in riser analysis by several researchers [12-14]. Wang et al. [15] presented a procedure for static analysis, where the riser is modelled as a large displacement beam under vertical and lateral loads in a vertical plane. The resulting system of nonlinear equations is solved using the Finite Difference Method (FDM).

Steel Catenary Risers (SCR) are one of the most effective options for deep water exploration [16], allowing large diameter export or production from remote wells [17]. Although the free-hanging catenary configuration is the simplest to install and connect with other subsea facilities, there are engineering issues related to high hang-off tension levels when the suspended length is large [18] and fatigue issues at the touchdown zone (TDZ).

To overcome these challenges, other riser concepts have been developed, such as Steel Lazy-Wave Risers (SLWR), in which buoyancy modules are added to a riser section, reducing the top loads and improving the fatigue life [19]. Wang et al. [20] proposed a mathematical model based on the large displacement beam theory to investigate the influences of internal flow and ocean current on SLWR, and to simulate a SLWR abandonment and recovery. FDM is used to solve the nonlinear differential equations.

This work presents a simple approach for riser analysis based on the differential equilibrium equations of a cable subjected to vertical and horizontal loads. This procedure considers the static loads acting on the riser and the vessel motions (static offsets). The resulting nonlinear Boundary Value Problem (BVP) is solved using the Newton-Raphson Method with line searches to increase efficiency and robustness. The bending moment is evaluated in a post-processing step using the riser curvature and bending stiffness. The accuracy and efficiency of the proposed approach is demonstrated comparing the obtained results for different riser configurations with those obtained with

a commercial FE software for riser analysis. It is important to note that when FDM or FEM are adopted, the number of equations increases when the mesh is refined, which leads to higher accuracy and the computational cost. On the other hand, the number of equations to be solved in the proposed approach is constant, ensuring its computational efficiency.

The rest of the paper is organized as follows. Section 2 describes the external loads considered by the analysis model and Section 3 presents the governing equations of the riser model. Section 4 presents the analysis algorithm and Section 5 describes the post-processing techniques. The numerical results are presented and discussed in Section 6. Finally, the concluding remarks are presented in Section 7.

2 Loads

Marine risers are subjected to several static loads, including self-weight, buoyancy, hydrostatic pressure, currents and floater movements (static offset). The direct loads acting on the riser will be discussed here, while the consideration of static offset will be discussed in Section 4.

The effective (or apparent) weight (w_e) corresponds to the resulting vertical load acting on the riser:

$$w_e = w_r + w_f - w_a \tag{1}$$

where w_r is the riser self-weight (or dry weight), w_f is the internal fluid weight and w_a is the buoyancy force, corresponding to the weight of the displaced seawater. According to Sparks [21], the effects of the hydrostatic pressure can be considered using the effective tension (T_e). Conceptually, the effective tension represents the axial force that balances the apparent weight of the riser, allowing submerged risers to be analyzed as cables outside the water. After the analysis, the true tension (T_t), which corresponds to the axial stresses on the riser wall, can be computed from:

$$T_t = T_e + p_i A_i - p_e A_e \tag{2}$$

where p_e is the external pressure, A_e is the external area, p_i is the internal pressure and A_i is the internal area.

The effect of the sea currents can be evaluated using the Morison approach [21], where a circular cylinder submerged in some fluid whose velocity is perpendicular to the cylinder axis is subjected to a drag force (f_D) proportional to the square of fluid velocity. For a horizontal current velocity (v), as depicted in Figure 1, the drag force is given by:

$$f_D = \frac{1}{2}\rho\, C_D\, D\, v \sin(\theta)\, |v \sin(\theta)| \tag{3}$$

where ρ is the seawater density, CD is the drag coefficient and D is the riser outer diameter.

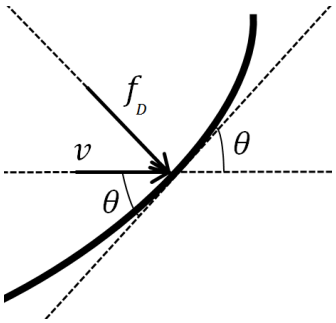

Figure 1. Current force.

3 Equilibrium Equations

The riser is modeled as an inextensible cable without bending stiffness, subjected to the effective

weight (w) and drag force (f_D). The governing equations of the model can be obtained from the equilibrium equations of the differential riser segment depicted in Figure 2.

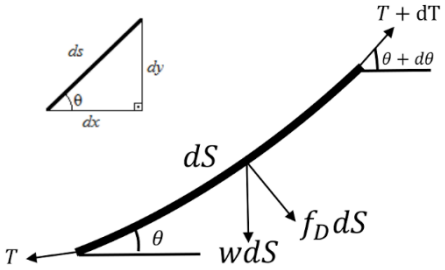

Figure 2. Loads on a differential segment.

The equilibrium equation in the axial direction can be written as:

$$(T + dT)\cos(d\theta) - T + w\sin\left(\theta + \frac{\mathrm{d}\theta}{2}\right)\mathrm{ds} + f_D\sin\left(\frac{\mathrm{d}\theta}{2}\right)\mathrm{ds} = 0 \tag{4}$$

While the equilibrium equation in the normal direction is given by:

$$w\cos\left(\theta + \frac{d\theta}{2}\right)ds - f_D\cos\left(\frac{d\theta}{2}\right)ds + (T + dT)\sin(d\theta) \tag{5}$$

These equations can be simplified considering $\cos(d\theta) = \cos(d\theta/2) = 1$, $\sin(d\theta) \cong d\theta$ and $\sin(d\theta/2) \cong d\theta/2$. Thus, neglecting the higher order terms, Eq. (4) can be rewritten as

$$dT + w\sin(\theta)ds = 0 \tag{6}$$

while Eq. (5) can be rewritten as:

$$Td\theta + w\cos(\theta)ds - f_D ds = 0 \tag{7}$$

It is important to note that the tension (T) considered in the above equations corresponds to the effective tension, since this is the tension that balances the effective weight (w). Eq. (6) and Eq. (7) describe the variation of the tension (T) and slope (θ) of the riser, respectively. In order to complete the set of governing equations is necessary to include the geometric relations:

$$\begin{aligned} dx &= ds\cos(\theta) \\ dy &= ds\sin(\theta) \end{aligned} \tag{8}$$

Therefore, the system of governing equations of the riser can be written as:

$$\begin{cases} \dfrac{dT}{ds} = -w\sin(\theta) \\ \dfrac{d\theta}{ds} = \dfrac{\frac{1}{2}\rho C_D D v\sin(\theta)|v\sin(\theta)| - w\cos(\theta)}{T} \\ \dfrac{dx}{ds} = \cos(\theta) \\ \dfrac{dy}{ds} = \sin(\theta) \end{cases} \tag{9}$$

It is important to note that the current velocity v can vary with the vertical coordinate y, while the parameters w, D and C_D can vary with the position s along the riser, as occurs in lazy wave configurations and other risers with multiple segments.

Equation (9) describes the behavior of suspended risers and to model SCRs and lazy wave configurations, it is necessary to model the riser-soil interaction. In order to obtain an efficient analysis procedure, the seabed is considered to be rigid, frictionless and horizontal. Therefore, the equilibrium equation for the riser segment in contact with the seabed is given by:

$$f_S = w \tag{10}$$

where f_s is the vertical soil reaction. Therefore, the governing equations describing the riser on the seabed are:

$$\begin{cases} \dfrac{dT}{ds} = \dfrac{d\theta}{ds} = \dfrac{dy}{ds} = 0 \\ \dfrac{dx}{ds} = 1 \end{cases} \tag{11}$$

4 Analysis Procedure

The riser static behavior is governed by nonlinear system of ordinary differential equations defined by Equations (9) and (11). The riser boundary conditions are prescribed in two points: the connection (initial point) and the anchor (final point). Thus, a two-point boundary value problem solution is required. In these problems, the boundary conditions at the beginning do not determine a unique solution to start with, and a random choice that satisfies these incomplete boundary conditions probably will not satisfy the boundary condition in the end [22], therefore the problem herein presented is complex. In this work, this Boundary Value Problem (BVP) will be efficiently solved using the Shooting Method.

Since there are four differential equations, four boundary conditions are required to solve the BVP. It is important to note that the connection coordinates (x_{con}, y_{con}), which are the coordinates of the point where the riser is connected to the vessel, are already known. For the consideration of floater movements (offsets), a simple adjustment of (x_{con}, y_{con}) to the new coordinates (riser position considering the static offset) is made. On the other hand, the top traction (T_{con}) and top angle (θ_{con}) are unknown. In this work, these values (T_{con} and θ_{con}) are estimated in order to transform this two-point boundary value problem into an initial value problem.

The user can define the initial values of T_{con} and θ_{con} as input data (Warm Start) or these initial values are estimated from the riser data (Automatic Shooting). When a riser is analyzed with different offsets and currents, the automatic shooting can be used to obtain the Mean configuration (i.e. without offset and current), while the results for this configuration can be used as warm start for other configurations (e.g. Near and Far). This approach improves both the efficiency and robustness of the numerical procedure.

The fourth-order Runge-Kutta method [22] is used in the numerical integration of the resulting initial value problem. In this method, the integration interval is divided in a number of steps, and the present step values are used in the calculation of the variables in the next step. Increasing the number of steps improves the integration accuracy, but also the computational cost. This issue will be assessed in the numerical examples.

For SCRs and lazy-wave risers, the integration procedure checks if the riser slope is zero, in this case it switches from Equation (9) to Equation (11). For lazy wave risers, the switch occurs only after the segment with negative effective weight. The procedure handles riser with multiple segments, as lazy wave riser. In this case, the integration is carried out segment-by-segment, where the initial values of segment *i*+1 corresponds to the final values of segment *i*.

After the integration, the coordinates of the final point (x_{fin}, y_{fin}) are obtained. These coordinates have to match with the prescribed coordinates of the anchor point (x_{anc}, y_{anc}). However, as the initial values of T_{con} and θ_{con} do not correspond to the exact values, a difference between (x_{fin}, y_{fin}) and (x_{anc}, y_{anc}) exists. Thus, the initial estimate must be improved in order to minimize the error on the final coordinates:

$$\mathbf{F} = \begin{bmatrix} x_{fin} - x_{anc} \\ y_{fin} - y_{anc} \end{bmatrix} = \mathbf{0} \tag{12}$$

which depends on the values of the initial variables:

$$\mathbf{V} = \begin{bmatrix} T_{con} \\ \theta_{con} \end{bmatrix} \tag{13}$$

In this work, Equation (12) is solved using the Newton-Raphson method, where the initial estimative $\mathbf{V_0}$ is updated iteratively as:

$$\mathbf{V}_{k+1} = \mathbf{V}_k + \delta\mathbf{V} \tag{14}$$

where the iterative correction $\delta\mathbf{V}$ is calculated solving the linear equations system:

$$\mathbf{J}\,\delta\mathbf{V} = -\mathbf{F} \tag{15}$$

In this equation, $\mathbf{J}$ is the Jacobian matrix:

$$J_{ij} = \frac{\partial F_i}{\partial V_j} \tag{16}$$

Since the analytical expressions of the vector $\mathbf{F}$ components are unknown, the derivatives that form the Jacobian matrix are approximated by the finite difference method. The iterative process continues until:

$$\frac{|\mathbf{F}|}{F_{norm}} \leq TOL \tag{17}$$

where F_{norm} is a normalization factor, considered as the distance between the connection and anchor points, and TOL is a prescribed tolerance.

The Newton-Raphson method has quadratic convergence near its solution, but it can diverge if $\mathbf{V_0}$ is far from the actual solution [22, 23]. Therefore, a line search procedure is used in this work to stabilize the iterative process and guarantee the global convergence of the solution method. The vector $\delta\mathbf{V}$ generated by Equation (15) is a descending direction that minimizes the residual $|\mathbf{F}|$ if a sufficiently small step is taken [22, 23]. Therefore, the line search procedure adopted in this work consists in replacing Equation (14) by the expression:

$$\mathbf{V}_{k+1} = \mathbf{V}_k + \alpha_l\,\delta\mathbf{V} \tag{18}$$

where α represents the step size that will be taken in $\delta\mathbf{V}$ direction. In order to preserve the quadratic convergence rate, it is initially considered that $\alpha_0 = 1$. It is checked if the new solution $\mathbf{V}$ reduces the error and if this does not occur, the step size is halved:

$$\alpha_{l+1} = \frac{\alpha_l}{2} \tag{19}$$

The process is repeated until the error becomes smaller than the previous iteration (k) error. In addition, the line search procedure also checks if the top tension (T_{con}) is positive, since a negative tension does not have physical meaning. The analysis algorithm is depicted in Figure 3.

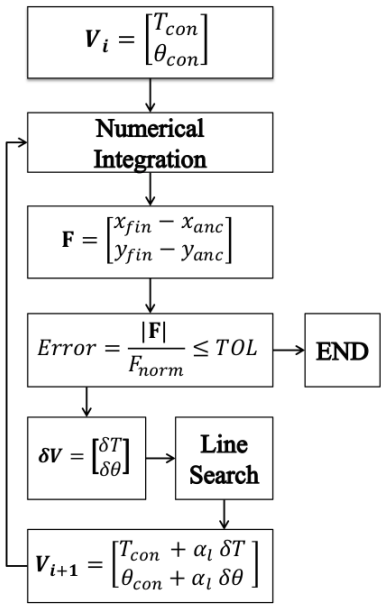

Figure 3 - Analysis algorithm.

5 Post-processing

From the differential geometry, the riser curvature κ can be computed using:

$$\kappa = \frac{d\theta}{ds} \tag{20}$$

which corresponds to the second line of Equation (9). It is important to note, that this curvature and an approximation of the true curvature of the riser, since the proposed model does not consider bending. In this work, the approximate curvature will be used to estimate the bending moment along the riser using the classical relation from the beam theory:

$$M = EI\,\kappa \tag{21}$$

where EI is the riser bending stiffness. Good results are expected, since the curvature values of a flexible cable are very close to the curvatures of a riser subjected to the same loads, except close to the end points [21]. The accuracy of this approach will be assessed in Section 6 .

The von Mises stress can be used to assess the safety of steel structures under complex stress states, due to hydrostatic pressure, axial force and bending moment. For a point in the riser wall, the von Mises stress (σ_{vm}) is given by

$$\sigma_{vm} = \sqrt{\frac{(\sigma_{tw} - \sigma_c)^2 + (\sigma_c - \sigma_r)^2 + (\sigma_r - \sigma_{tw})^2}{2}} \tag{22}$$

where σ_{tw} is the axial stress, σ_c is the hoop stress and σ_r is the radial stress. In this work, the von Mises stress is evaluated at 4 points in the riser cross-section, as shown in Figure 4, which assumes that the bending moment is applied on the section x-axes.

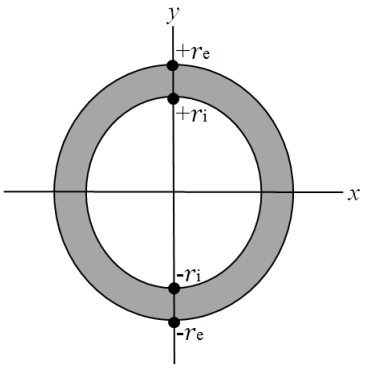

Figure 4. Riser cross-section.

The true axial stress in the pipe wall (σ_{tw}) including the effect of the bending moment is given by:

$$\sigma_{tw} = \frac{T_{tw}}{A_e - A_i} \pm \frac{Mr}{I} \tag{23}$$

in which I is the moment of inertia of the riser cross-section. The other stress components (σ_c and σ_r) can be easily obtained from the internal and external hydrostatic pressure [21].

6 Numerical Examples

The formulation presented in the previous sections was implemented in C++ and used to analyze risers with different configurations. The obtained results are compared with FE results obtained with FLEXCOM [24], a FE software widely used in the offshore industry.

In all numerical examples, the relative perturbation adopted for numerical differentiation is 10^{-6} and the tolerance for convergence (TOL) is 10^{-8}. The water density is 1025 kg/m³ and the gravity acceleration is 9.81 m/s². For the automatic shooting option, the initial top angle was considered as 20º (θ_0 = -70º = -7π/18 rad) and the connection tension was estimated as $T_0 = W/(1.5 \sin\theta_0)$, where W is the total effective weight of the riser.

6.1 Hanging riser

This example corresponds to a riser hanged at both ends and subjected to its own weight. This example does not consider current effects and was previously studied in other works [11, 25]. It was initially used to validate the formulation and the implementation of the analysis model herein presented, and later to investigate the influence of the bending stiffness on the riser behavior. Additional riser data is presented in Table 1.

Table 1. Riser data.

x_c(m)	0.0
y_c(m)	0.0
x_a(m)	150.0
y_a(m)	150.0
S (m)	350.0
w (N/m)	346.094
D (m)	0.26
EI (N.m²)	2.096E+04

Table 2 summarizes the results obtained with the cable model presented in this work and with FEM, both considering 50 divisions (or elements). Two different FE models were utilized, the first one considering the bending stiffness given in Table 1 (beam model) and the second one using a bending stiffness close to zero, aiming to disregard the bending effects (i.e. truss model). As it will be shown, the comparison of the results obtained using truss and beam elements indicates that the bending stiffness does not influence significantly the top traction and top angle values when a mesh with proper refinement is considered.

Table 2. Results of the hanging riser with 50 divisions.

Model	**Tension (N)**	**Diff. (%)**	θ_{con} **(deg)**	**Diff. (%)**	M_{max} **(Nm)**	**Diff. (%)**
Beam	3.592×10^4		19.232		630.977	
Truss	3.592×10^4	0.004	19.224	−0.04	−	−
Cable	3.592×10^4	−0.01	18.571	−3.44	634.060	0.49

Due to the large difference between the top angles obtained with N_{div} = 50, the riser was analyzed with different meshes and the obtained results are presented in Table 3. The results show that the cable model is more accurate when the number of divisions is small, but the difference decreases with the mesh refinement. The mesh refinement also led to a smaller difference for the maximum bending moment. Thus, for N_{div} = 100 the difference decreased from 0.49% to 0.10%, with the bending moment of the FEM approaching of the results of the model proposed herein, whose value was kept constant.

Table 3. Top angle (θ_0).

N_{div}	Beam	Cable	Diff. (%)
50	19.232	18.571	−3.44
100	18.913	18.571	−1.81
150	18.817	18.571	−1.31
200	18.775	18.571	−1.09
250	18.751	18.571	−0.96
300	18.738	18.571	−0.89
350	18.729	18.571	−0.85

The riser geometry obtained with the three models is shown in Figure 5. It is noted that the geometry obtained in the proposed formulation is very close to the one obtained by FEM. Figure 6 shows the tension along the riser for the different models, and once again the comparison shows that the results are in very good agreement. These results show that the bending stiffness has little influence on the geometry and tension in static models.

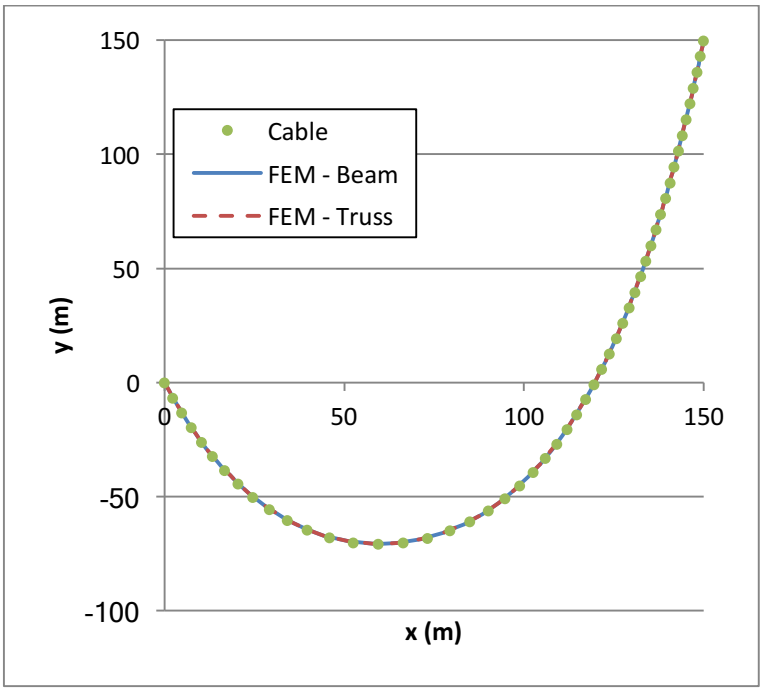

Figure 5. Hanging riser geometry.

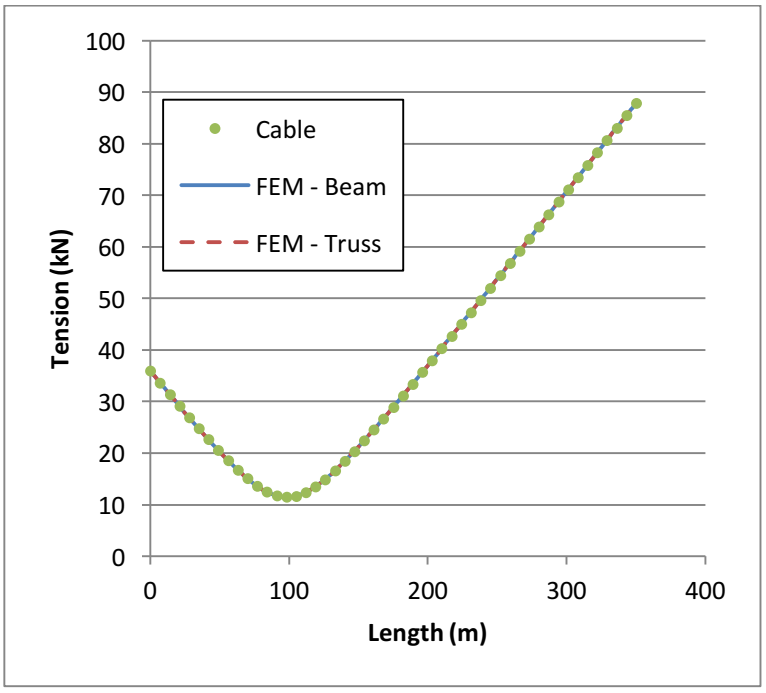

Figure 6. Tension in the hanging riser.

A comparison between the bending moments obtained by FE beam model and by the proposed cable model is presented in Figure 7. The results are in excellent agreement for the entire riser length, showing the adequacy of the post-processing approach presented in Section 5 .

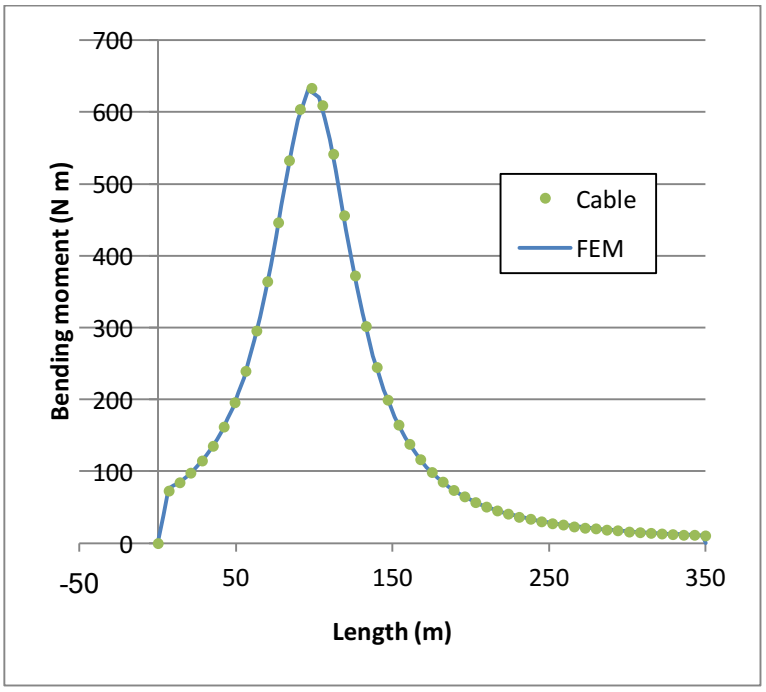

Figure 7. Bending moment in the hanging riser.

Figure 8 presents a comparison of the CPU time for each analysis model. Since the proposed model is simpler than FEM, the execution time of the analyses is lower. It is interesting to note that the time computation increases linearly with the number of divisions and the advantage of the proposed approach increases with refinement.

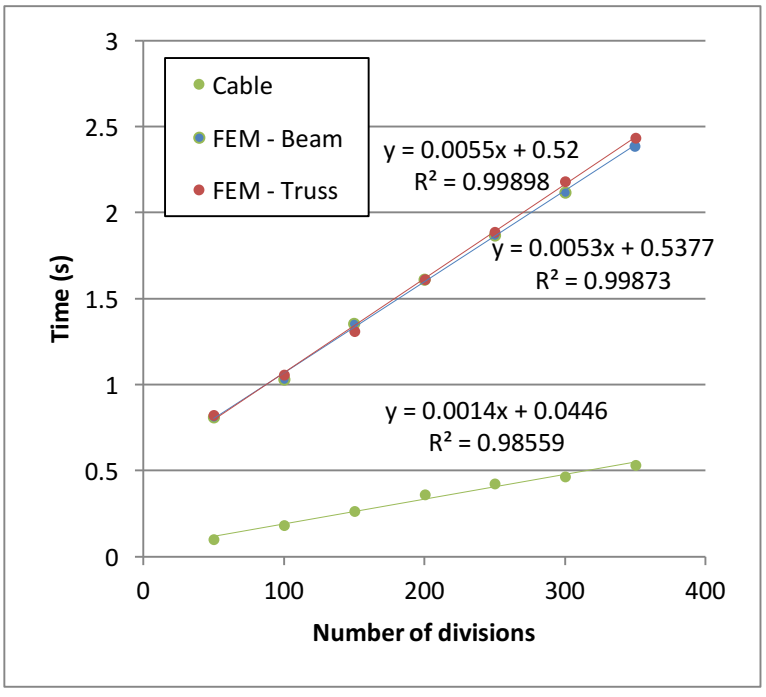

Figure 8. CPU time for the hanging riser.

6.2 Steel Catenary Riser

This example considers a Steel Catenary Riser (SCR) subjected to its apparent weight and a piecewise linear current profile, corresponding to the Far configuration [24]. The relevant parameters are presented in Table 4. Additional parameters used only by the finite element model are presented in Table 5.

Table 4. SCR data.

x_c(m)	-94.5
y_c(m)	1173.9
x_a(m)	1200.0
y_a(m)	0.00
S(m)	1955.0
w (N/m)	1323.5
V_0 (m/s)	0.0
V_{1091} (m/s)	-0.15
V_{1136} (m/s)	-0.30
V_{1181} (m/s)	-0.45
C_D	1.2
D (m)	0.273
EI (N/m²)	3.18E+07

Table 5. Parameters used only by the FE model.

Axial friction coefficient	0.2
Lateral friction coefficient	0.4
Vertical soil stiffness (kN/m²)	143.4
Longitudinal soil stiffness (N/m²)	45
Transverse soil stiffness (N/m²)	90

Results for tension and top angle using the three previously mentioned models (FE/Beam, FE/Truss and Cable) are presented in Table 6. For comparison purposes, 98 divisions are considered for the three models, with this mesh, each element measures approximately 20 m. As in the first example, the differences are very small, corresponding to 0.1% for top tension and 2.29% for the maximum bending moment.

Table 6. SCR results.

Model	**Tension (N)**	**Diff. (%)**	θ_{con} **(deg)**	**Diff. (%)**	M_{max} **(Nm)**	**Diff. (%)**
Beam	2.206×10^6		17.184		6.575×10^4	
Truss	2.206×10^6	0.01	17.202	0.10	–	–
Cable	2.209×10^6	0.14	17.201	0.10	6.425×10^4	2.29

Riser geometry and tension along its length are presented in Figure 9 and Figure 10, respectively. This example is more complex than the previous one, since this SCR is subjected to environmental loads (offset and current), however, the results were again in very good agreement.

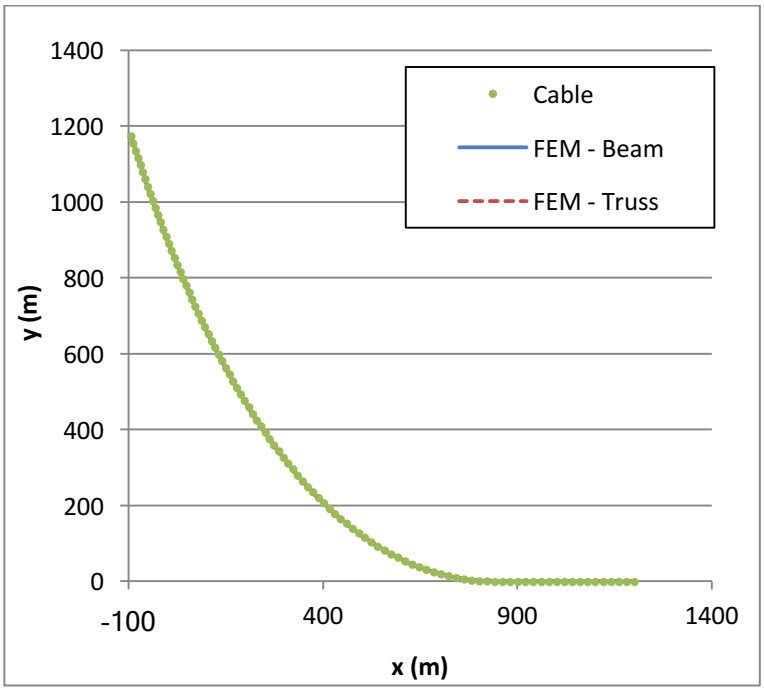

Figure 9. SCR geometry (Far).

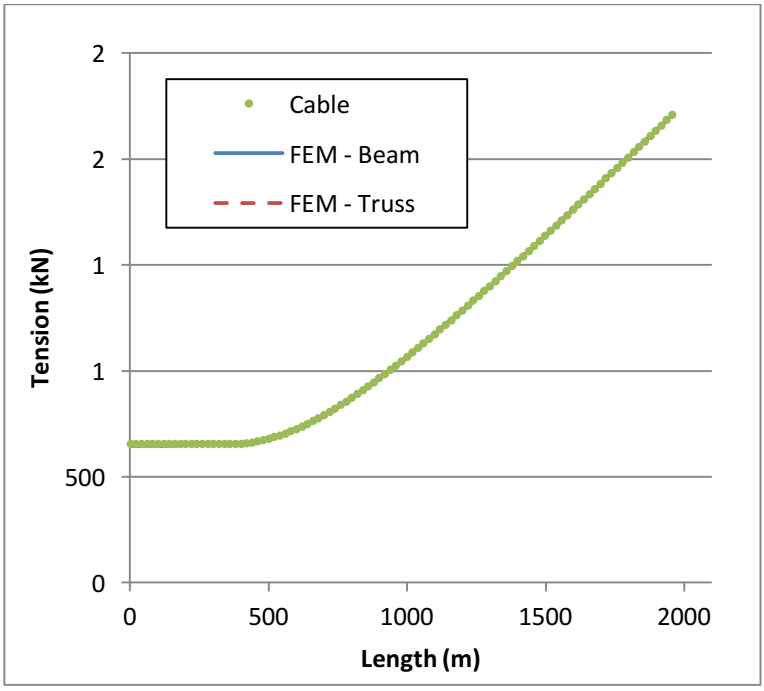

Figure 10. SCR - Tension.

Figure 11 shows the bending moments along the riser length evaluated by the FEM and by the proposed cable model. Excellent agreement is obtained for the entire riser, except at the touchdown zone (TDZ), which is expected due to the large curvature variation in this region and the different riser-soil interaction models used by each approach. Nevertheless, by doubling the number of divisions, the maximum bending moment is 64217 Nm for the cable and 63943 Nm for the FE model, and the difference between them reduces from 2.29% to 0.04%. Comparing the results with the previous refinement, it is possible to note that the cable model had already presented good results with a coarser discretization. This emphasizes the greatest advantage of the model herein presented: it is

quicker and more accurate than the FEM, since it needs less refinement to converge, and for any refinement, it is quicker, as previously noted.

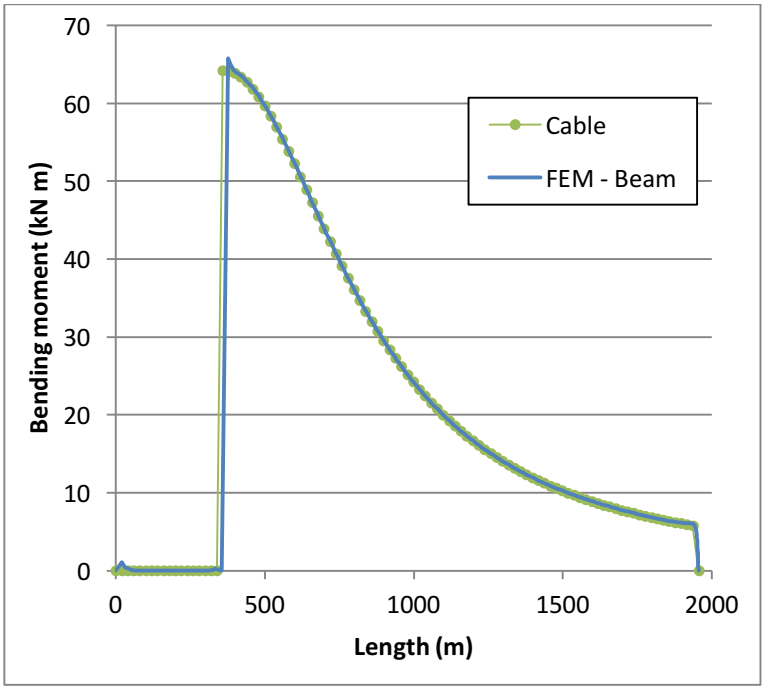

Figure 11. SCR - Bending moment.

The von Mises stresses along the riser length computed using FEM and the proposed cable model are presented in Figure 12. The results present an excellent agreement, where the difference between the maximum values is only -0.08%.

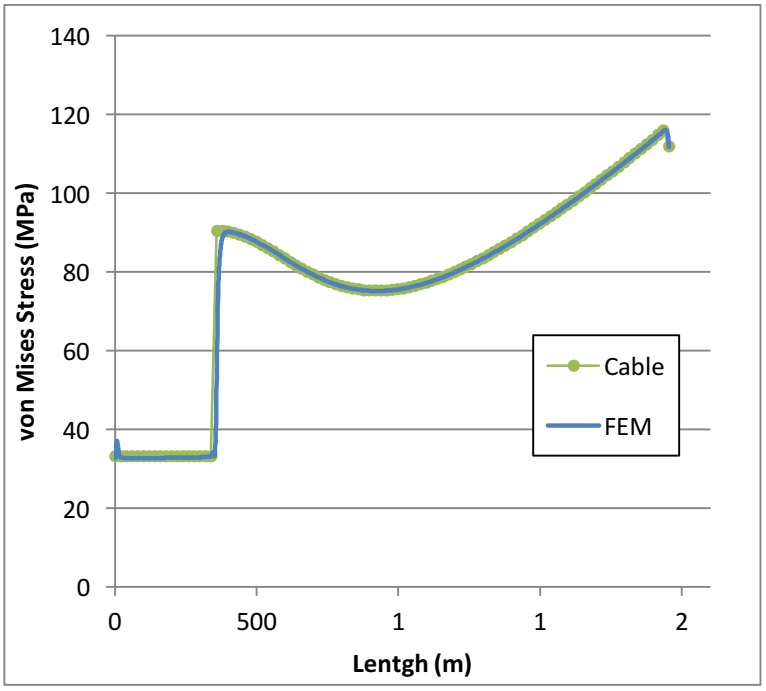

Figure 12. SCR – von Mises stress.

It is important to note that the finite element model considers a flex-joint and an I-tube at the connection [24]. Even without considering these components and considering a rigid seabed, the

proposed model was capable of obtaining satisfactory results, proving its effectiveness.

6.3 Steel Lazy Wave Riser

In this example, the SLWR studied by Orimolade [26] is analyzed in the Mean, Far and Near configurations. The vessel offset is 110 m and the riser is subjected to a piecewise linear current profile. Other riser parameters are presented in Table 7. For comparison purposes, 210 divisions are considered for the three models, each element measuring 10 m. Additional parameters used only by the finite element model are presented in Table 8.

Table 7. SLWR data.

x_c(m)	0
y_c(m)	1088.0
x_a(m)	1320.0
y_a(m)	0
S_1(m)	1239.0
S_2(m)	441.0
S_3(m)	420.0
ρ_o (kg/m³)	800
$\rho_{aço}$ (kg/m³)	7850
w_1, w_3 (N/m)	1069.4
w_2 (N/m)	-700
V_0 (m/s)	0.23
V_{450} (m/s)	0.23
V_{610} (m/s)	0.39
V_{775} (m/s)	0.54
V_{950} (m/s)	0.83
V_{990} (m/s)	1.05
V_{1030} (m/s)	1.31
V_{1088} (m/s)	1.67
C_D	1.0
D_{o1}, D_{o3} (m)	0.304
D_{o2} (m)	0.758
D_i (m)	0.254
E (N/m²)	2.070E+11
I (m^4)	2.149E-04

Table 8. Parameters used only by the FE model.

Internal pressure (MPa)	34.5
Axial friction coefficient	0.3
Lateral friction coefficient	0.5
Vertical soil stiffness (kN/m²)	50
Longitudinal soil stiffness (kN/m²)	200
Transverse soil stiffness (kN/m²)	200

The comparisons of the results obtained for tension, top angle and maximum bending moments for the mean, far and near configurations are included in Table 9, Table 10 and Table 11. For these configurations, the errors are low and the influence of the bending stiffness is very small. The obtained riser geometries are illustrated in Figure 13.

Table 9. SLWR results in configuration Mean.

Method	Tension (N)	Diff. (%)	θ_{con}(deg)	Diff. (%)	M_{max} (Nm)	Diff. (%)
Beam	1.223×10^{6}	-	7.999	-	2.759×10^{5}	–
Truss	1.224×10^{6}	0.07	8.032	0.41	–	–
Cable	1.224×10^{6}	0.09	8.028	0.37	2.784×10^{5}	0.91

Table 10. SLWR results in configuration Near.

Method	Tension (N)	Diff. (%)	θ_{con}(deg)	Diff. (%)	M_{max} (Nm)	Diff. (%)
Beam	1.200×10^{6}	-	9.456	-	3.937×10^{5}	–
Truss	1.201×10^{6}	0.07	9.667	2.23	–	–
Cable	1.202×10^{6}	0.23	8.401	11.2	4.050×10^{5}	2.87

Table 11. SLWR results in configuration Far.

Method	Tension (N)	Diff. (%)	θ_{con}(deg)	Diff. (%)	M_{max} (Nm)	Diff. (%)
Beam	1.269×10^{6}	-	8.126	-	1.844×10^{5}	–
Truss	1.269×10^{6}	0.01	7.984	1.75	–	–
Cable	1.267×10^{6}	0.15	9.066	11.6	1.874×10^{5}	1.57

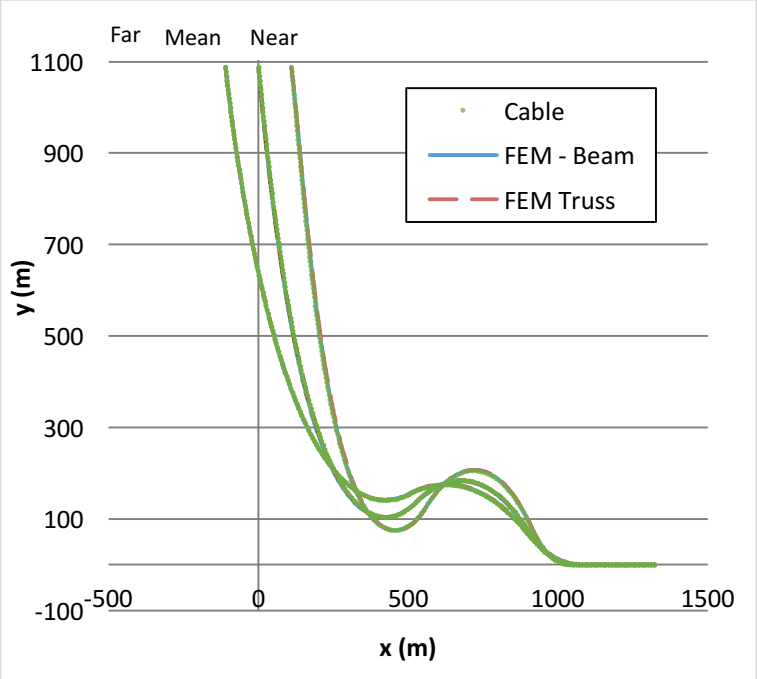

Figure 13. SLWR - geometry in the 3 different configurations.

The warm start and the linear search procedures were also studied in this example. The warm start was used to obtain the Near configuration, where the top tension and top angle used in the initial shoot were the ones obtained in the Mean configuration values (1223800 N; 0.140 rad), while the Mean configuration was obtained using the automatic shooting. It is shown in Table 12 that the program

needs less iterations to converge when the warm start is used, and also that when the initial shoot is far from the solution, which occurs in the automatic shooting in this example, the linear search acts, helping the method to achieve its convergence. The method did not converge when the linear search was not used in the same example.

Table 12. Warm start and linear search validation.

	Automatic Shooting		**Warm Start**	
Iteration	**Error**	**α**	**Error**	**α**
1	4.92×10^{-1}		7.16×10^{-2}	
2	1.76×10^{-1}	0.5	2.53×10^{-3}	1.0
3	2.19×10^{-2}	1.0	1.52×10^{-5}	1.0
4	7.17×10^{-4}	1.0	6.36×10^{-10}	1.0
5	1.23×10^{-6}	1.0	-	-
6	3.65×10^{-12}	1.0	-	-

The comparisons for tension and bending moment obtained in the Far position with the three procedures are presented in Figure 14 andFigure **15**, respectively. The tension values obtained with the proposed model were again very satisfactory. Higher differences were found in the bending moment in the TDZ, due to the riser-soil interaction and the large variation of the riser curvature in this zone. However, it is important to emphasize that in all riser points, the bending moments were always higher on the cable model, indicating that the proposed model lead to slight conservative results.

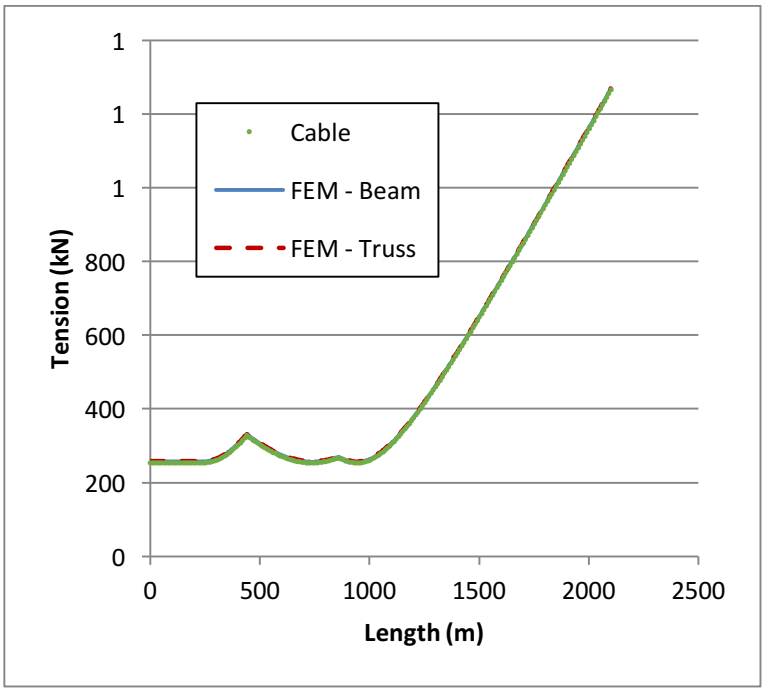

Figure 14. Tension - SLWR.

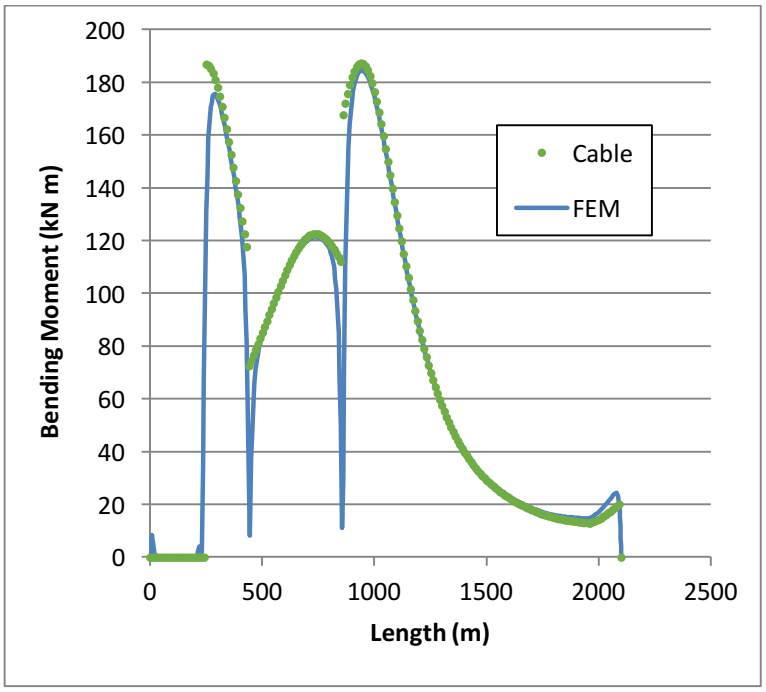

Figure 15. SLWR - Bending moment.

The von Mises stresses were evaluated on the Near and Far configurations. As shown in Figure 16, the differences are very small, except for the TDZ. In fact, the differences between the maximum values were 0.04% for the Near and 0.01% for the Far configuration. It is important to note that the riser geometry in the Near configuration is more complex, since the curvature sign changes faster, leading to larger bending moment differences. However, the differences are small, with the proposed approach leading to slightly conservative results.

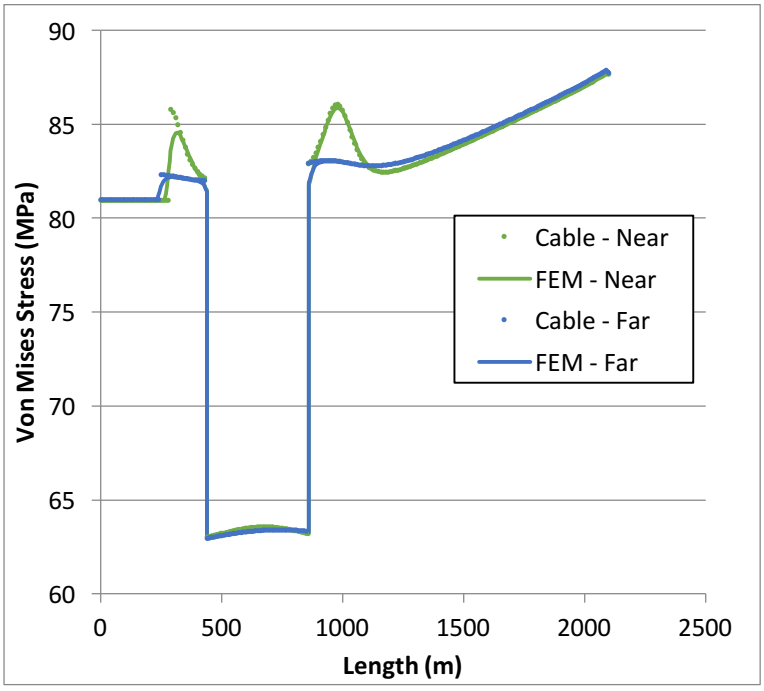

Figure 16. SLWR – von Mises Stress.

7 Conclusion

This work presented a simple approach for riser analysis based on the differential equilibrium equations of a cable subjected to static loads. This procedure considers the static loads acting on the riser and the vessel motions. An efficient and robust solution algorithm is adopted to solve the resulting nonlinear equations. The bending moment is evaluated in a post-processing step using the riser curvature and bending stiffness.

Different riser configurations were analyzed and compared to the results obtained with a FEM program in order to validate this model. The results for geometry, tension, and bending moment and von Mises stresses were very accurate. The results showed that the proposed formulation is not only more efficient than FEM for the same discretization, but also requires a coarse discretization to converge, resulting in an accurate and efficient approach for static analysis, especially in the early design phases where many different options and configuration have to be assessed.

Acknowledgements

The financial support by CNPq (Conselho Nacional de Desenvolvimento Científico e Tecnológico) and by ANP/UFC PRH-31 (Agência Nacional do Petróleo) is gretefully acknowledged.

References

[1] Rustad, A.M.; LarsenC.M., SørensenA.J. FEM modelling and automatic control for collision prevention of top tensioned risers. Marine Structures, vol. 21, pp. 80–112, 2008.
[2] Det Norske Veritas, Offshore Standard DNV-OS-F201: Dynamic Risers, 2010.
[3] Chakrabarti, S.K.; Frampton R.E.; Review of riser analysis techniques. Applied Ocean Research, vol. 4, pp. 73-90, 1982.
[4] Patel, M. H.; Seyed, F. B.; Review of flexible riser modelling and analysis techniques. Engineering Structures, vol. 17, n. 4, p. 293-304. (1995)
[5] Zhan J. P.; Review and verification of marine riser analysis programs. Thesis (MSc), NTNU. (2010)
[6] Quéau L. M.; Kimiaei M.; RandolphM.F.; Analytical estimation of static stress range in steel catenary risers at touchdown area and its application with dynamic amplification factors. Ocean Engineering. Vol. 88, pp. 63–80, 2014.
[7] Lima, B. S. L. P.; Jacob, B. P.; Ebecken, N. F. F.; A hybrid fuzzy/genetic algorithm for the design of offshore oil production risers. International Journal for Numerical Methods in Engineering. vol. 64, p. 1459-1482, 2005.
[8] Jacob B., Vieira I. N., Silva A. J. M.; de Lima B. S. L. P.; A comparative study applied to risers optimization using bio-inspired algorithms. International Journal of Modeling and Simulation for the Petroleum Industry, vol. 38, 2009.
[9] Pina, A. A.; Albrecht, C. H.; Lima, B. S. L. P.; Jacob, B. P.;Tailoring the Particle Swarm Optimization algorithm for the design of offshore oil production risers. Optimization and Engineering, vol. 12, n. 1-2, p. 215-235.(2010)
[10] Silva, R. F., Teófilo, F. A. F., Parente, E., de Melo, A. M. C., & de Holanda, Á. S.; Optimization of composite catenary risers. Marine Structures, 33, 1-20, 2013.
[11] Ghadimi, R. A simple and efficient algorithm for the static and dynamic analysis of flexible marine risers. Computers and Structures, 1988
[12] Chai, Y. T.; Varyani, K. S.; Barltrop, N. D. P.; Three-dimensional Lump-Mass formulation of a catenary riser with bending, torsion and irregular seabed interaction effect. Ocean Engineering, vol. 29, pp. 1503-1525, 2002.
[13] Pollio, A.; Marano, G. C.; Mossa, M.; Langley, R. L.; Low, Y. M.; A Comparison of Time Domain and Frequency Domain Analysis of a Flexible Marine Riser Undergoing Large Deformations

by Using a Lumped Mass Approach. Proceedings of the Sixteenth International Offshore and Polar Engineering Conference, 2006.
[14] Zhu, K.; Zheng, D.; Cai, Y.; Yu, C.; Wang, R.; Liu, Y.; Zhang, F.; Nonlinear hydrodynamic response of marine cable -body system under random dynamic excitations. Journal of Hydrodynamics, Ser. B, vol. 21, pp 851-855, 2009.
[15] Wang Y.; Gao D.; Fang J.; Static Analysis of deep-water marine riser subjected to both axial and lateral forces in its installation. Journal of Natural Gas Science and Engineering, vol. 19, pp 84-90, 2014.
[16] Howells, H. Advances in steel catenary riser design, DEEPTEC'95, Aberdeen, UK, 1995.
[17] Campbell, Mike. The complexities of fatigue analysis for deepwater risers. Proceedings of the deepwater pipeline conference, New Orleans. 1999.
[18] Wang, J. L.; Duan M.L.; A nonlinear model for deepwater steel lazy-wave riser configuration with ocean current and internal flow. Ocean Engineering, vol. 94, pp. 155–162, 2015.
[19] Thomas B., Benirschke A., Sarkar T., 2010. Parque das conchas (BC-10) steel lazy wave riser installation pre abandonment, recovery and transfer challenges. In: The 2010 Offshore Technology Conference.
[20] Wang, J.; Duan, M.; Luo, J.; Mathematical model of steel lazy-wave abandonment and recovery in deepwater. Marine Structures., vol. 41, pp. 127–153, 2015. http://dx.doi.org/10.1016/j.marstruc.2015.02.002
[21] Sparks, C.P. Fundamentals of Marine Riser Mechanics. Penn Well, 2007.
[22] Press, W. H., Teukolsky, S. A., Vetterling, W. T. Flannery, B. P. Numerical Recipes: The Art of Scientific Computing. Third Edition, Cambridge University Press, (2007).
[23] Dennis J. E.; Schnabel R.B.; Numerical Methods for Unconstrained Optimization and Nonlinear Equations. SIAM, Philadelphia, 1996.
[24] MCS Kenny, Theory Manual, Flexcom Version 8.1, Galway Technology Park, Galway, Ireland 2012.
[25] McNamara, J. F.; O'Brien, P. J.; Gilroy, S.G.; Non-linear analysis of flexible risers using hybrid finite elements. OMAE, 1986.
[26] Orimolade, Adekunle Peter. Steel lazy wave risers from turret moored FPSO. MS thesis. University of Stavanger, Norway, 2014.